Geomechanics and Engineering, *Vol. 16, No. 1 (2018) 35-47*
DOI: https://doi.org/10.12989/gae.2018.16.1.035

Rock fracturing mechanisms around underground openings

Baotang Shen*[1,2] and Nick Barton[3a]

[1]*College of Mining and Safety Engineering, Shandong University of Science and Technology, 579 Qianwangang Road, Huangdao District, Qingdao, Shandong Province, 266590, China*
[2]*Commonwealth Scientific and Industrial Research Organization (CSIRO) Energy, P.O. Box 883, Kenmore, Brisbane QLD 4069, Australia*
[3]*Nick Barton & Associates, Fjordveien 65c,1363 Høvik, Oslo, Norway*

(Received August 17, 2017, Revised February 26, 2018, Accepted March 13, 2018)

Abstract. This paper investigates the mechanisms of tunnel spalling and massive tunnel failures using fracture mechanics principles. The study starts with examining the fracture propagation due to tensile and shear failure mechanisms. It was found that, fundamentally, in rock masses with high compressive stresses, tensile fracture propagation is often a stable process which leads to a gradual failure. Shear fracture propagation tends to be an unstable process. Several real case observations of spalling failures and massive shear failures in boreholes, tunnels and underground roadways are shown in the paper. A number of numerical models were used to investigate the fracture mechanisms and extents in the roof/wall of a deep tunnel and in an underground coal mine roadway. The modelling was done using a unique fracture mechanics code FRACOD which simulates explicitly the fracture initiation and propagation process. The study has demonstrated that both tensile and shear fracturing may occur in the vicinity of an underground opening. Shallow spalling in the tunnel wall is believed to be caused by tensile fracturing from extensional strain although no tensile stress exists there. Massive large scale failure however is most likely to be caused by shear fracturing under high compressive stresses. The observation that tunnel spalling often starts when the hoop stress reaches 0.4*UCS has been explained in this paper by using the extension strain criterion. At this uniaxial compressive stress level, the lateral extensional strain is equivalent to the critical strain under uniaxial tension. Scale effect on UCS commonly believed by many is unlikely the dominant factor in this phenomenon.

Keywords: tunnel spalling; fracture propagation; extension strain criterion; shear fracturing; failure mechanism; FRACOD

1. Introduction

Rock masses are increasingly employed as the host medium in a vast array of human activities. Facilities like storage caverns, petroleum wells, water and transport tunnels, and underground power stations are located in a variety of rock types and suffer extra challenges when at significant depth. Excavation stability is imperative for all such constructions, in both the short and long term. The understanding of fracturing of rock masses has become a necessity for deep rock excavations in brittle rocks. Small-scale breakouts around single wells in petroleum engineering help to indicate principal stress direction and the degree of stress anisotropy. Large-scale stress-or-strain induced fracturing in tunnels can lead to massive tunnel failure which not only increases the time and cost of tunnel excavation and maintenance, but also imposes serious safety threats to personnel, and occasionally leads to fatalities.

Failure of brittle rock is often associated with explicit fracturing events. The mechanisms of rock fracturing around an actual underground excavation are often complex and have been constantly debated amongst researchers. Tunnel spalling is the most commonly observed fracturing phenomenon in highly stressed brittle rock, and most researchers believe it is caused by tensile fracturing (Andersson 2007, Martin and Chandler 1994). However, researchers have been struggling to explain convincingly why tensile fracturing occurs in the tunnel wall where no tensile stress exists. Also difficult to explain is that the spalling tends to start when the maximum estimated hoop or tangential stress reaches approximately 0.4*UCS (Uniaxial Compressive Strength) (Martin *et al.* 1999). Some researchers tend to believe this may be a logical scale effect on UCS. However, this phenomenon not only occurs in large scale tunnels but also in laboratory scale samples (Martin 1997), making the scale effect theory inadequate.

Large scale massive failures have been observed in tunnels and boreholes under very high stresses (Barton 2006). This is believed to be caused predominately by shear fracturing. Fracturing around boreholes drilled at various angles into a highly-stressed brittle medium in the laboratory (not a thick-walled cylinder test) was consistently caused by the log-spiral shear mechanism (Addis *et al.* 1990).

Diederichs (2003) and Diederichs *et al.* (2004) carried out detailed studies on the mechanisms of rock fracturing in hard rocks, and believed that, depending on the stress state, failure could be caused by shear (high confining stress), spalling (low confining stress) or tension (tensile stress), see

∗Corresponding author, Professor
E-mail: baotang.shen@csiro.au
[a]Professor

http://www.techno-press.org/?journal=gae&subpage=7
ISSN: 2005-307X (Print), 2092-6219 (Online)

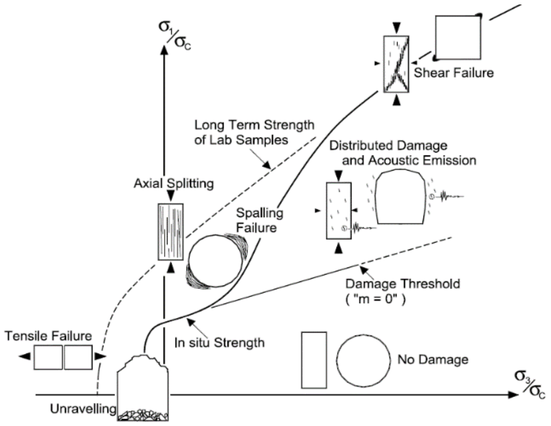

Fig. 1 Schematic of failure envelope for brittle failure, showing four zones of distinct rock mass failure mechanisms: no damage, shear failure, spalling, and unraveling. σ_c is the unconfined compressive strength (UCS) of laboratory samples. (After Diederichs 2003)

Fig. 1. They also investigated the mechanisms believed to be causing the lower (than UCS) spalling strength at zero or low confining stress, and suggested that the observed spalling stress/strength ratio (0.35-0.45) could be contributed by microcrack initiation and interaction.

Various new studies on the mechanisms of tunnel failure have been conducted recently by researchers around the world. Huang *et al.* (2017) performed a laboratory investigation of the fracturing mechanisms in a granite sample with two holes under a Brazilian-type test. Wang *et al.* (2017) carried out a field monitoring study of the splitting failures in the side walls of large scale underground caverns. Chen *et al.* (2016) performed a numerical study to predict the failure zones in coal in a deep underground coal mine roadway. Li *et al.* (2016) investigated the micro- and macro- fracturing mechanisms in deep tunnels affected by horizontal bedding. Komurlu *et al.* (2015) attempted to predict numerically the effect of in-situ stresses on the failure zones surrounding a circular underground tunnel. All these studies have greatly helped to improve our understanding on the failure mechanisms around underground excavations.

This paper investigates the mechanisms of tunnel spalling and massive tunnel failures using fracture mechanics principles. The study starts by examining the fracture propagation due to simple tensile and shear failure mechanisms. Several real case observations of spalling failures and massive shear failures in boreholes, tunnels and underground roadways are shown in the paper. The extension strain criterion has been discussed in detail in this paper and it has been used to explain the tunnel spalling mechanism and the “0.4*UCS” phenomenon. Numerical models were used to investigate fracture mechanisms in the roof/wall of a deep tunnel and in an underground coal mine roadway.

2. Fracture propagation mechanisms

In the case of hard massive rocks where brittle behaviour is dominant, failures can be induced by fracture initiation and propagation. When the principal induced stress in the rock mass is high enough, which is often 40-50% of the intact rock strength, fracture initiation will occur. Fracture initiation could occur from the existing defects in the rock mass such as pores, flaws, or micro-cracks. Fracture initiation however does not necessarily mean that the rock mass is losing its bearing capacity and will collapse. When a rock mass is under compressive stresses, the fractures are more likely to grow in a stable manner toward the direction of the major compressive stress. This process is often a stable process as it needs incremental stresses to maintain fracture propagation. The predominant mechanism of fracture propagation at this stage is tensile (or mode I). At a later stage when the induced stress is close to the ultimate strength of the rock, shear (or mode II) fracture propagation will occur. Shear fracturing is often an unstable process. Once initiated it can propagate very rapidly in the direction of maximum shear stress and minimum shear resistance. The strain energy released from the fracture propagation will not be dissipated adequately by the fracture friction and fracture surface energy. The excessive energy may then become the kinetic energy which causes rocks to be displaced in a dynamic manner to the opening.

The stable and unstable fracture propagation in initially intact rock can be clearly demonstrated by the case shown in Fig. 2, where one single inclined fracture in an infinite rock mass is under uniaxial compression. This figure shows the results from a simple numerical model using a fracture mechanics code FRACOD (Shen *et al.*, 2014). Details of this code will be given in the following sections of this paper. With a sufficiently high stress, the pre-existing fracture will propagate in tension (mode I) in a curved path toward the direction of the loading stress (Fig. 2(a)). This is typically the wing crack formation often referred to in fracture mechanics. However, as the fracture grows in this manner, the strain energy released due to the crack tip extension is gradually reducing, as shown in Fig. 2(c). This means that to maintain fracture growth, the stress needs to be increased gradually. Because the stresses in the rock mass are generally pre-existing, rather than increasing this type of fracture propagation will only extend to a limited distance before ceasing, unless driven for instance, by neighboring mining-face advance. No significant levels of kinetic energy release is expected from the stable tensile fracture growth.

In contrast, when the fracture is to propagate in shear as shown in Fig. 2(d), the fracture extends in the general direction of the shear failure plane which is close to the original fracture plane. As the fracture grows in length, the strain energy released is actually increasing (Fig. 2(f)). The excessive energy released in the system will not only drive the fracture growth very rapidly but also cause the kinetic energy release. This mechanism may lead to violent failure in a highly stressed (and strained) rock mass, if it is sufficiently massive i.e., sparsely jointed before such an event.

The stress condition is the key factor for the type of fracture propagation. Under a uniaxial compressive stress, fractures are most likely to propagate in tension initially,

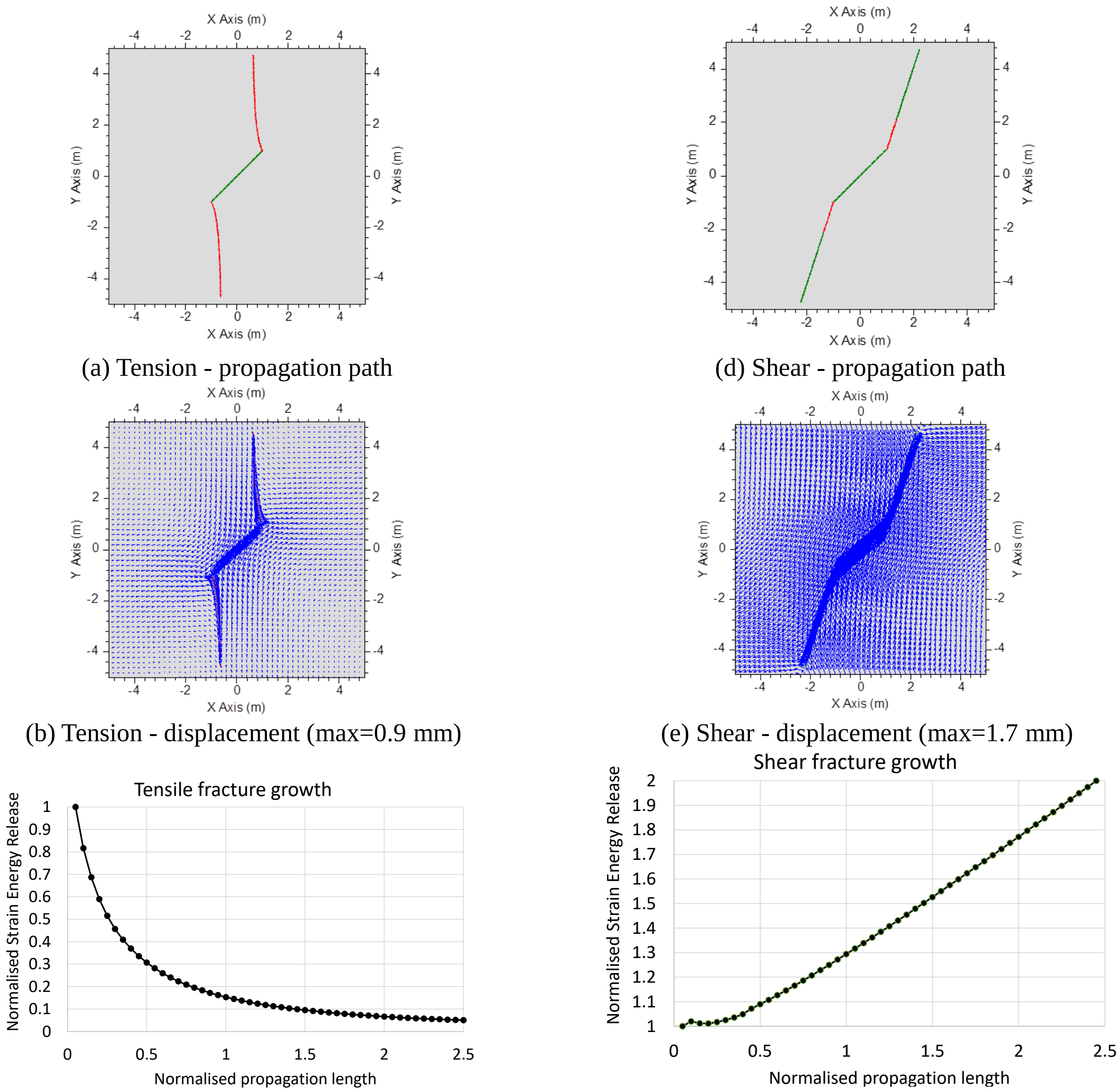

(a) Tension - propagation path

(d) Shear - propagation path

(b) Tension - displacement (max=0.9 mm)

(e) Shear - displacement (max=1.7 mm)

(c) Tension - strain energy release rate

(f) Shear - strain energy release rate

Fig. 2 Fracture propagation in tension or shear under uniaxial compression in the vertical direction. (a) and (c)-Tensile (mode I) fracture propagation leads to decreasing energy release and hence stable fracturing; (d) and (f)-Shear (mode II) fracture propagation results in increasing energy release and hence unstable fracturing. Note that the path of shear fracturing is highly dependent on the fracture roughness and dilation. The case in (d) is for a smooth pre-existing fracture and secondary fractures without dilation which is the worst-case scenario for dynamic failure. The rock displacement resulting from tensile and shear fracture propagations in (b) and (e) is quite different. Shear fracturing causes a much larger rock displacement than tensile fracturing

with the possibility of shear failure at a later stage. Under a bi-axial or tri-axial compressive stress condition, tensile fracturing is unlikely due to the lack of tensile stresses in the rock mass, unless the proximity of a free surface allows the minimum stress to be significantly lower than the major principle stress, in which case extension fracturing, due to the effect of Poisson's ratio, can occur as tensile failure. Without the nearby free surface, fractures are more likely to propagate in shear and the energy release will be higher due to the high stress condition needed to trigger such rock fracturing.

In fact rock properties can determine whether failures will be in a violent manner or not. It is commonly known that brittle rock such as granite can fail violently in laboratory compression tests with the samples bursting at the peak load. Coal is also a brittle material, and fails violently, although its strength is of course much less than granite, so energy dissipation is much less, but it is serious and may be dangerous to personnel at in situ scale.

The brittle behaviour of rock has been classified into two types: Class I and Class II (Fig. 3) according to Wawersik and Fairhurst (1969), based on the post-peak characteristics of its full loading-unloading curve from (servo-controlled) laboratory uniaxial compression tests. For class I, fracture propagation is stable, in the sense that the work must be done on the sample for each incremental decrease in load-carrying capacity. The sample will only fail by continued movement of the machine platens. For class

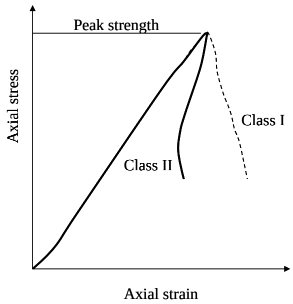

Fig. 3 Rock types are classified into Class I and Class II in view of the post-peak axial deformation behaviour Modified from Wawersik and Fairhurst (1966)

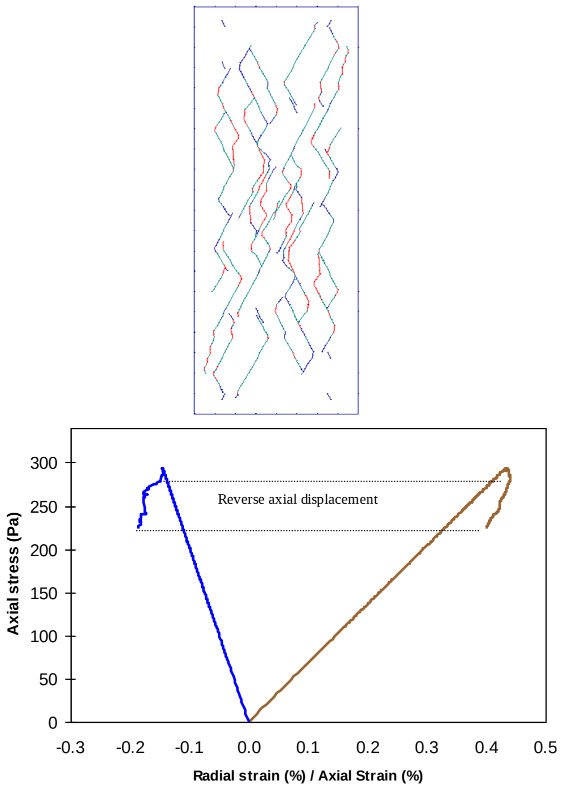

Fig. 4 Modelled fracturing pattern (top) and axial and radial stress-strain curves (bottom) for Äspö rock which exhibits Class II type of rock behaviour (After Rinne, 2008). In the numerical model, the rock is assumed to be isotropic and a linearly elastic material before fracturing. Hence the initial stage of nonlinear behaviour due to microcrack closure as observed in Fig. 3, is not simulated. The predicted fracture initiations started in the central part of the model with many isolated fractures. With increasing load, these fractures coalesce and eventually form several large failure planes. Fracture colour: red-open; light blue-shear; dark blue-elastic contact

II, failure is unstable or self-sustaining. To control the fracture, elastic energy must be extracted from the material. Class II rocks will continue to fail just after the peak, if the strain is maintained constant (fixed platen displacement). To control the fast failure process the surplus strain energy must be significantly removed from the system by moving the loading plates in a reversed direction. Obviously Class II type of rock is more likely to induce violent failure in the laboratory, and is a potential rockburst candidate around a highly stressed rock excavation.

Class II behaviour was successfully tested on Äspö diorite rock in the laboratory at Aalto University in Finland (Rinne 2008), and was also captured numerically using the fracture mechanics based code FRACOD (Shen *et al.* 2014), as shown in Fig. 4. In both the laboratory tests and numerical model, unloading was started after passing the peak strength using strain reduction. Understanding the fracturing mechanisms, either in a stable or violent manner, is the key to predict rock failure at different scales.

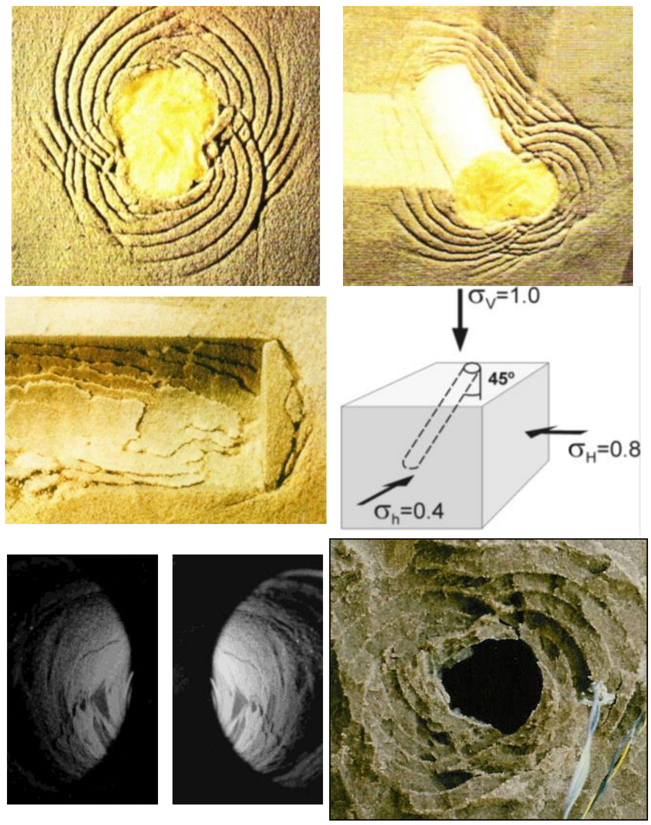

Fig. 5 Obvious log-spiral shearing in model tunnels/well-bores, which were drilled into highly-stressed blocks (0.5 × 0.5 × 0.5 m) of weak model sandstone. All three principal stresses could be varied independently through flat-jack loading, and drilling did not need to be parallel to any of the principal boundary stresses. The upper four photographs show the results of stress anisotropy and hole deviation from the horizontal. The lower two photographs show tests in a smaller polyaxial cell in which hole drilling was parallel to the minimum horizontal stress. Miniature monitoring boreholes and pressure cells were installed before drilling under stress. Coloured cemented sand in pre-drilled boreholes confirmed that 'log-spiral' shearing does indeed involve shear displacements. Tensile/extensional modes were not evident in these physical model studies, which might be due to the high level of confining stress, which was several times the magnitude of UCS. (After Addis *et al.* (1990), Barton and Shen (2017))

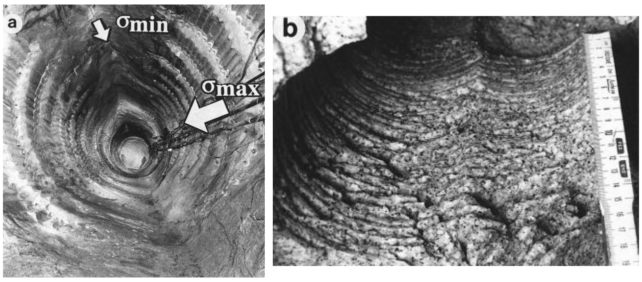

Fig. 6 (a) Tunnel breakout and (b) observed tensile spalling close to the face at the URL mine-by tunnel experiment in Manitoba, Canada where AECL researchers conducted a very gradual excavation by line-drilling so as to be able to observe the processes as closely as possible. (After Read and Martin 1996, Martin 1997).

Fig. 8 A coal burst event at Austar Mine, Australia. The coal rib burst out during roadway development. The overburden depth was 550 m (NSW Mine Safety Investigation Unit, 2015).

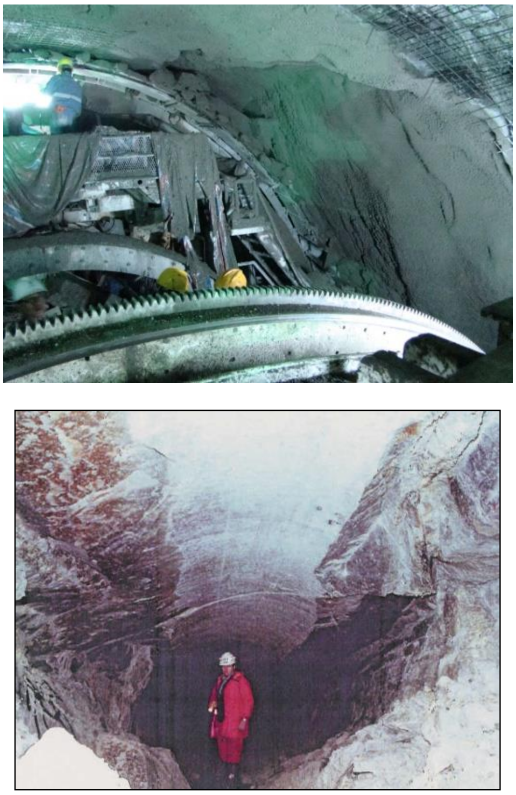

Fig. 7 Two tunnel failure cases. Top-a limited dynamic failure in Jinping II Tunnel in medium strength marble, China. Bottom-failure in the early (1880) Beaumont Tunnel in (5-10 MPa) chalk-marl, close to the UK Channel Tunnel. (After Barton and Shen (2017))

3. Rock Fracture mechanisms around underground openings

In highly stressed rock masses, excavations such as boreholes, tunnels and mining roadways may create critical levels of stress redistribution and concentration in the vicinity of the opening. Typically the radial stress in the roof/wall of the opening will be reduced to near zero whereas the tangential stress will be significantly elevated. The maximum tangential stress, for instance in the arch and invert, will be several times higher than the *in situ* stress. In the immediate roof/wall of the opening, uniaxial (or biaxial) compressive conditions exist due to the removal of the confining stress. Further away from the roof/wall however, tri-axial compressive stress conditions still exist because the radial stress increases with distance into the rock, and still acts as a confining stress.

The stress redistribution and concentration near the deep excavation may cause rock mass failure in the form of distinct fracturing. This will be more distinct when the natural jointing is sparse or absent. Two very different failure modes have been observed, both of them ‘physical realities’ but from very different environments. The first is from petroleum wellbore simulations in sandstones. With change of scale, a small deep tunnel in a weak but brittle rock can be envisaged. Failure is dominated by (log-spiral) shearing (Fig. 5). The second is a real case involving highly-stressed granite in an underground research laboratory: the Underground Research Laboratory (URL) in Canada. Initiation is by tensile/extensional fracturing, but there is shearing and buckling, and the development of a final characteristic notch (see Fig. 6).

In many real rock engineering failures, particularly those involving extensive rock or coal burst, the fracturing mechanisms are often complex and both tensile and shear fracturing are involved. Fig. 7 shows two cases of massive failures in highly stressed TBM tunnels. The upper photo shows the aftermath of a moderate rock burst of Jinping II tunnel in China at a depth of approx. 1 km. When at greater depth (at least 2 km) a major rockburst event in the pilot TBM cost several lives to be lost. The lower photo is from the earliest (1880) Beamont pilot tunnel close to the 1990’s UK Channel Tunnel in chalk marl. A 70 m increase in the depth of cover, where the tunnel passed under a sea cliff, caused the massive shear failure.

Fig. 8 shows a coal burst failure that occurred at Austar Mine in Australia on April 15, 2014, which resulted in two fatalities. The coal rib of an underground roadway heading suddenly burst out during roadway development. The failed coal is confined vertically by the Dosco Stone Band within the Greta Coal Seam. The smooth and dominant shear surface presented by the Dosco Stone Band appears to have acted as a dynamic shear failure plane. The mechanisms of

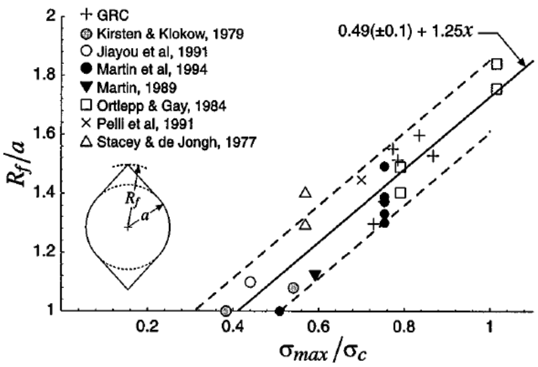

Fig. 9 Observations of failure initiation and depth of 'stress-induced' over-break (after Martin *et al.* 1999). The common stress/strength ratios for spalling are in the range of 0.3 - 0.5 with a medium value of approximately 0.4. In reality the critical 'stress/strength' ratio 0.4 is related to critical tensile strain, and the typical ratios of σ_c/σ_t, as demonstrated using Eqs. (1)-(3)

the coal failure in the main rib are unclear, but it is highly likely that mixed shear and tensile fracturing have occurred

It has been recognised that both tensile (or extensional strain induced) fracture initiation and propagation in shear have their important roles to play. Tensile initiation may consist of critical strain-initiated extensional fracturing, which can explain several puzzling phenomena such as tensile fracturing in entirely compressive stress fields (e.g., Fairhurst and Cook 1966). In a recent study, Barton and Shen (2017) used the extension strain criterion to investigate tunnel failure mechanisms. This paper will provide the fundamental details of the extension strain criterion, and its implementation into a numerical code: FRACOD, for modelling engineering problems. Based on the extension strain theory, which was originally developed by Stacey (1981) and later extensively discussed by Wesseloo and Stacey (2016). If the strain in a direction becomes tensile and reaches a critical value, tensile fracturing will occur. The original extension strain theory, however, uses the "critical strain" as the measure of failure which is not commonly tested in the laboratory, and it does not link explicitly with the known parameters (such as tensile strength σ_t). In this paper we will establish a stress-based formula using the extension strain theory.

A two-dimensional *plane-strain* equation for expressing extensional strain (in the lateral direction) is as follows

$$\varepsilon_3 = (1-\nu^2)/E\ [\sigma_3 - \nu\sigma_1] \qquad (1)$$

where ν is the Poisson's ratio of the intact rock and E is the Young's modulus.

From Eq.(1), extensional strain may develop in a stress field where both principal stresses are compressive, due to the effect of Poisson's ratio. This explains why tensile fracturing can occur in the roof/wall of an underground opening where no tensile stress is expected. The only requirement will be that $\nu\sigma_1 > \sigma_3$, i.e., the disparity between the major principal stress (σ_1) and the minor principal stress (σ_3) needs to be high enough.

The critical extensional strain (ε_t) for tensile fracturing can be determined using the tensile strength of the rock (σ_t) when a rock specimen is under unaxial tension (σ_1=0; $\sigma_3=\sigma_t$), i.e.,

$$\varepsilon_t = (1-\nu^2)\sigma_t/E \qquad (2)$$

Using the critical extensional strain in Eq. (2) to replace ε_3 in Eq. (1) we obtain the critical compressive (i.e., tangential) stress for tensile fracturing (or spalling) to occur

$$\sigma_1(\text{spalling}) = (\sigma_t + \sigma_3)/\nu \qquad (3)$$

Considering that the confining stress σ_3 is zero at the wall of an underground opening, then for rocks with typically UCS ≈ $10\sigma_t$ and Poisson's ratio ≈ 0.25, tensile fracturing will start when the uniaxial (or tangential) stress reaches ≈ 0.4*UCS. Interestingly many rock engineers, mining engineers and researchers have observed that tunnel spalling starts when the maximum tangential stress (σ_θ) at the tunnel wall reaches around 0.4±0.1*UCS (e.g., Martin *et al.* 1999), as shown in Fig. 9. Similar phenomon have been found independently by Barton and Grimstad (2014) who reproduced the historic (pre-1990) case records from Grimstad, which show that ratios of σ_θ/σ_c were mostly in the range 0.4-0.8 for road tunnels of 600 to 1,400m depth where 'stress-slabbing' (extensional strain) and rock burst (shear failures) had occurred. These were the reason for strongly increased SRF in the Q-system tunnel support recommendations, for the case of massive rock (Grimstad and Barton 1993, Barton and Shen 2017).

Extension-strain theory may in fact be the best explanation for field observations of tunnel spalling at lower stress levels, rather than the mobilization of UCS. However, this is at odds with the belief by many that the lower spalling strength was caused by a scale effect on UCS. Many researchers have demonstrated in the laboratory that rock strength can reduce significantly with size (e.g., Hoek and Brown, 1980). Some researchers (e.g., Dresen *et al.*, 2010) found that the borehole spalling stress is strongly size dependent when the borehole size is less than 20mm but becomes less size dependent for borehole size greater than 20mm and the borehole spalling strength converges to a constant. Cai and Kaiser (2014) reviewed many previous laboratory borehole failure (mostly hollow-cylinder) studies and stated that "although scale-dependent behaviour was observed for smaller holes, the failure hoop stress was almost identical to the uniaxial compressive strength when the hole diameter was greater than 75 mm". According to our latest studies, the scale effect on fracture initiation may not be the key mechanism causing the lower spalling strength than UCS for tunnels on the engineering scale. We believe that tunnel spalling is a result of tensile fracturing due to excessive extensional strain caused by the uniaxial/biaxial compression stress state as the tunnel wall is approached.

Tensile fracturing and spalling may be the start of a failure process at the early stage but it is unlikely to be the root cause of massive failure. Further away from the wall/roof of an underground excavation, the confining stress (σ_3) will be higher and the major principal stress will be lower due to the moderation of stress concentration with distance from the opening. Hence, tensile fracturing conditions may not be met anymore. In this region, shear fracturing driven by high shear stress will be dominant. In

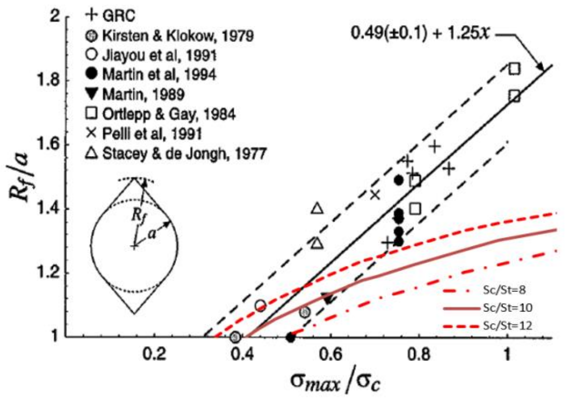

Fig. 10 Comparison of the estimated tunnel break-out depth using extension strain theory (red solid and dash lines) with the observed results from deep tunnels and mines (black solid and dash lines and black data points).

other words massive shear failures, not tensile failures, are needed to explain the observations at higher stress levels

To demonstrate this effect, we consider a circular tunnel in a massive rock mass with far-field stresses σ_1 and σ_3. In the rock mass along the direction of major principal stress σ_1 the tangential and radial stress can be expressed as

$$\begin{aligned} \sigma_\theta &= \frac{\sigma_1+\sigma_3}{2}\left(1+\frac{a}{r}\right)+\frac{\sigma_1-\sigma_3}{2}\left(1+3\frac{a^2}{r^2}\right) \\ \sigma_r &= \frac{\sigma_1+\sigma_3}{2}\left(1-\frac{a}{r}\right)-\frac{\sigma_1-\sigma_3}{2}\left(1-\frac{a}{r}\right)\left(1-3\frac{a}{r}\right) \end{aligned} \tag{4}$$

where σ_θ and σ_r are the tangential stress and radial stress, respectively; a is the tunnel radius; r is the distance to tunnel centre. We will try to determine the depth of tensile spalling caused by extensional strain in the tunnel wall and its relationship with the ratio of tangential stress and UCS (σ_{max}/σ_c) as used in Fig. 9.

Assuming the far-field stress $\sigma_1 = 2\sigma_3$ and Poisson's ratio ν=0.25, we examined three cases with different rock compressive strength to tensile strength ratios: σ_c/σ_t = *8, 10, 12.* Using Eq. (3) and Eq. (4), it is possible to obtain the depth of spalling caused by the excessive extensional strain, which is actually the distance (r) where the extensional strain reached the critical value. For any given far-field stress value σ_1 , the spalling distance (r) can be obtained from the solution of Eq. (5)

$$3\left(1+\frac{a}{r}\right)+\left(1+3\frac{a^2}{r^2}\right)=\left[\frac{4\sigma_t}{\sigma_1}+3\left(1-\frac{a}{r}\right)-\left(1-\frac{a}{r}\right)\left(1-3\frac{a}{r}\right)\right]\frac{1}{\nu} \tag{5}$$

Using the relation of $\sigma_{max} = 3\sigma_1 - \sigma_3 = 2.5\sigma_1$, Eq. (5) can also be expressed in terms of the ratio of maximum hoop stress to rock UCS (σ_{max}/σ_c) and the spalling-depth ratio (R_f/a) as used in Fig. 9.

$$\frac{\sigma_{\max}}{\sigma_c}=\frac{1}{10}\left(\frac{\sigma_c}{\sigma_t}\right)\bullet\left(\begin{array}{l} 3\nu\left(1+\left(\frac{R_f}{a}\right)^{-1}\right)+\nu\left(1+3\left(\frac{R_f}{a}\right)^{-1}\right) \\ -3\left(1-\left(\frac{R_f}{a}\right)^{-1}\right)+\left(1-\left(\frac{R_f}{a}\right)^{-1}\right)\left(1-3\left(\frac{R_f}{a}\right)^{-1}\right) \end{array}\right)^{-1} \tag{6}$$

Eq. (6) gives the relationship between the stress ratio (σ_{max}/σ_c) and the spalling depth/radius ratio (R_f/a) for a circular tunnel in an unjointed rock mass with far-field stress $\sigma_1 = 2\sigma_3$. It is obviously dependent on the ratio of rock compressive strength to tensile strength σ_c/σ_t and Poisson's ratio ν. For the commonly used value for brittle rock ν = 0.25 and σ_c/σ_t = 10±2, Eq. (6) gives the critical spalling stress/strength ratio of 0.4 ± 0.08. This is very close to the empirical value of 0.4 ± 0.1 reported by Martin (1997).

At higher stress ratio (σ_{max}/σ_c), the spalling depth will increase. The spalling ratios (R_f/a) calculated using Eq. (6) are plotted against the stress ratio (σ_{max}/σ_c) for the three σ_c/σ_t values in Fig. 10, and the curves are compared with the empirical linear envelopes provided by Martin *et al.* (1999). It can be noticed that for shallow spalling (e.g., R_f/a ≈1.0), Eq. (6) gives results similar to the empirical values. However, for extensive tunnel failure (e.g., R_f/a >1.2), the estimated tunnel failure depth using Eq. (6) based on the extension strain theory, does not agree with the observed failure depth, and it is much less than the actual observations. This suggests that for deep extensive tunnel failure, the failure mechanism is very different from the tensile fracturing. Note that Eq. (6) did not consider the stress redistribution caused by the progressive spalling failure, which could also increase the failure depth from the estimated values. As will now be demonstrated by numerical modelling, shear fracturing instead of tensile fracturing is the dominant failure mechanism for large scale extensive tunnel failure.

4. Modelling of massive failures using a fracture mechanics code

As discussed in the previous sections, massive rock failure is controlled by dynamic fracturing in brittle rocks where explicit fracturing rather than plasticity is the dominant mechanism of failure. Prediction of the explicit fracturing process is therefore necessary when the rock mass stability is investigated for engineering purposes. However, the fracture mechanics approach is seldom used in practical rock engineering design, partly due to the inadequate understanding of complex fracturing processes in jointed rock masses, and partly due to the lack of tools which can realistically predict the complex fracturing phenomenon in rock masses.

Since the 1990s, a new approach to simulating rock mass failure problems has been developed using a numerical code called FRACOD (Shen *et al.*, 2014). FRACOD is a code that predicts the explicit fracturing process in rocks using fracture mechanics principles. Over the past three decades, significant progress has been made in developing this approach to a level that it can predict actual rock mass stability at an engineering scale. The code also includes complex coupling processes between the rock mechanical response, thermal processes and hydraulic flow, making it possible to handle complex coupled problems often encountered in geothermal, hydraulic fracturing, nuclear waste disposal, and underground LNG storage. During this period, numerous cases have been modelled using FRACOD. These include: borehole stability in deep geothermal reservoirs, pillar spalling under mechanical and thermal loading; prediction of tunnel and shaft stability and excavation disturbed zones (EDZ), etc.

FRACOD is a two-dimensional code which is based on the Displacement Discontinuity Method (DDM) principles. In the FRACOD model, fractures are represented by a number of DD elements. When fracture propagation is detected, new DD elements will be added to the existing fracture tips to simulate fracture growth. The criterion used in FRACOD to detect fracture propagation is the F-criterion developed by Shen and Stephansson (1993). This criterion is capable of predicting both tensile (Mode I) and shear (Mode II) fracture propagation which is particularly useful for rock fracture propagation as both tensile and shear failure are common in rock masses. According to the F-criterion, in an arbitrary direction (θ) at a fracture tip there exists an F-value, which is calculated by

$$F(\theta) = \frac{G_I(\theta)}{G_{Ic}} + \frac{G_{II}(\theta)}{G_{IIc}} \tag{7}$$

where G_{Ic} and G_{IIc} are the critical strain energy release rates for mode I and mode II fracture propagation; $G_I(\theta)$ and $G_{II}(\theta)$ are strain energy release rates due to the potential mode I and mode II fracture growths when expressed in terms of unit length.

The direction of fracture propagation will be the direction where the F-value reaches the maximum value. If the maximum F value reaches 1.0, fracture propagation will occur.

FRACOD also predicts fracture initiation starting with intact rock. Because FRACOD considers the intact rock as a flawless and homogeneous medium, any fracture initiation from such a medium represents a localised failure of the intact rock. The localised failure will be predicted by the intact rock failure criterion.

A fracture initiation can be formed due to tension or shear. For tensile fracture initiation, the extension strain criterion discussed in the previous section and represented by Eq. (3) is used in FRACOD. The new rock fracture will be generated in the direction perpendicular to the maximum extensional strain. The length of the newly generated fracture can be specified by the user, or automatically defined by the code, based on the element length used for fractures and the spacing of the grid points used in the intact rock.

For a shear fracture initiation, the Mohr-Coulomb failure criterion is used. When the shear stress at a given point of the intact rock exceeds the shear strength of the intact rock, a new rock fracture will be generated in the direction of potential shear failure plane.

4.1 Modelling extensive failure in deep tunnels

FRACOD has been used recently to simulate several cases of deep tunnels, in order to investigate the mechanisms of tunnel spalling/failure. In all cases, an 8 m diameter tunnel excavation was simulated, first of all in an elastic and massive rock mass without joints. The in situ stress state in the 2D plane perpendicular to the tunnel cross-section was assumed to represent a stress ratio of σ_{Hmax}/σ_v=2.0 at simulated depths of 1,000 m and then 2000 m, both with and without joints.

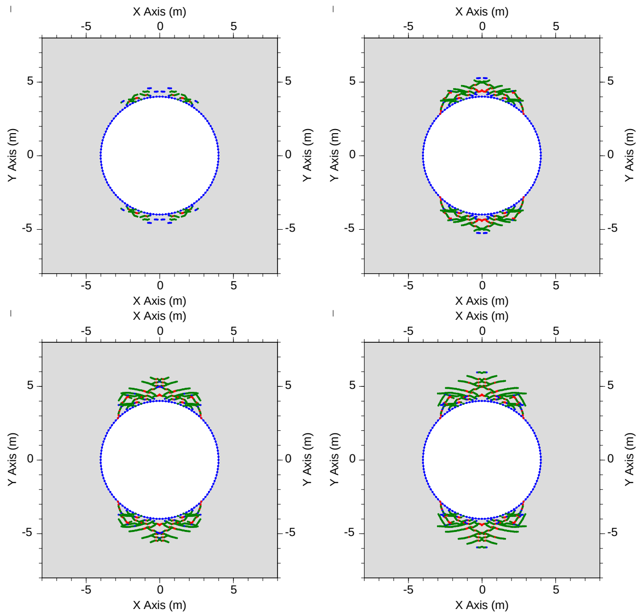

Fig. 11 A FRACOD model of a 1 km deep tunnel, showing some of the progressive stages of fracturing, first due to extensional-strain induced failure in tension (in red and blue) despite the compressive stress field, followed by log-spiral style (and connecting) larger-scale shearing (in green)

Model at 1000 m depth with and without joints

The numerical model has boundary stresses σ_{Hmax} = 50 MPa and σ_v = 25 MPa. For the base case, the strength and fracture toughness of the rock were: UCS = 165 MPa; cohesion c =31 MPa; internal friction angle ϕ=49°; tensile strength σ_t = 14.8 MPa; mode I fracture toughness K_{IC}=3.8 MPa $m^{1/2}$ and mode II fracture toughness K_{IIC}=4.7 MPa $m^{1/2}$. Fracture initiation length was set to be 0.2 m.

These parameters are the same as those of Äspö diorite, and are listed in the literature (e.g., Siren (2012) who compares Finnish and Swedish rocks). The maximum tangential stress at the tunnel was calculated to be σ_{max} = 125 MPa, and the ratio of σ_{max}/UCS is therefore 0.75. Based on Martin *et al.* (1999), the depth of tunnel failure (from Fig. 9) is R_f/a = 1.3-1.5. For the above case, the predicted failure process is shown in progression in Fig. 11. The key observations are:

• Fracture initiation occurred in the roof and floor where the compressive stress was the highest. The fracture initiation was driven by extensional strain due to the high compressive stress, and the initiated fractures were sub-parallel to the tunnel wall surface.

• The new short fractures were not predicted to propagate in tension because there is no tensile stress in the tunnel wall. FRACOD predicts that they propagate in shear, forming a kink path from the initial fractures, and they continue to propagate at an angle from the tunnel wall surface.

• As the propagation of the fractures near the tunnel wall progresses, new fractures continue to form deeper into the rock. These fractures also propagate in shear, eventually forming a larger (potential) breakout.

• The ratio of failure depth to tunnel radius (R_f/a) is predicted to be 1.5, which is close to the upper limit predicted by Martin *et al.* (1999).

Overall, the modelling results indicate that the fractures initiate due to extensional strain related failure-in-tension mechanisms. However, the dominant mechanism of tunnel failure is caused by a log-spiral style of shearing.

Fig.12 shows the three cases without joints and with one and two sets of joints.

Model at 2,000 m depth with and without joints

Three additional models were run, one without joint and two with joints. The models have the same geometry as shown in Fig. 12 but the rock strength is reduced by 50% and the *in situ* stresses are increased by 100% to simulate a tunnel in medium strong rock at a depth of 2 km. In very rough terms it could suggest that this approximates the very challenging conditions inevitably experienced at Jinping II in China, where four 16.6 km long headrace tunnels (plus transport and pilot tunnels) were driven through mountains giving an exceptional depth of cover of 2.0 to 2.5 km for several kilometers. However, the horizontal stress is exaggerated, deliberately, in order to emphasize possible fracturing effects.

The predicted failure patterns for the three models are shown in Fig. 13. For the model without joints, extensive fracturing occurred in the surrounding rock in the tunnel roof and floor where the failure depth showed $R_f/a > 1.5$. Nearly 70% of the tunnel surface was predicted to have extensive fracturing, and the fracturing was dominated by shearing. Laboratory experiments (e.g., Shen *et al.* 1995) and discussion in Section 2 indicate that shear fracturing in brittle materials tends to be very rapid and unstable. This is in contrast to tensile fracturing (e.g., wing cracks) under compression in which the crack growth is a pseudo-stable and progressive process, requiring increased boundary stresses for continued propagation.

The extensive and shear-dominated fracturing in this model implies that, at the depth of 2 km with high tectonic stress, large tunnels in medium-strong rock masses are likely to experience dynamic and massive failure, which could be intense like massive rock bursts.

The model with one joint set showed fracturing in the tunnel roof and floor extending more than 2m into the rock. However, the depth of expected breakout (where intensive fracturing leads to near complete rock mass failure) was limited to about $R_f/a = 1.25$-1.38. In the case of the model with two joint sets at closer spacing, fracturing in the tunnel roof and floor was even more limited. Several new fractures occurred in the rock blocks in the roof and floor, but their propagation was terminated when meeting the existing joints. This model further demonstrates the effect of joints on tunnel breakout. Joints are playing a positive role in reducing the stress concentration and hence reducing the fracturing in the surrounding rock. At shallow depth, joints have other roles.

4.2 Modelling extensive roadway failure in underground coal mines

Several models have been used to simulate the rib failure around a roadway heading in an underground coal mine. The roadway has a rectangular shape with a size of 5 m (width) and 3 m (height). The coal seam has a thickness of 3 m, and it is assumed to be overlain and underlain by massive sandstone units. The roadway is at a depth of 500m with *in situ* stresses $\sigma_{Hmax} = \sigma_v = 12.5$ MPa. The strength and fracture toughness of the rock and coal are: Coal: UCS = 10 MPa; cohesion c = 2.3 MPa; internal friction angle ϕ = 41°; tensile strength σ_t = 0.1 MPa; mode I fracture toughness KIC = 0.1 MPa $m^{1/2}$ and mode II fracture toughness K_{IIC} = 0.3 MPa $m^{1/2}$, Young's modulus E = 2.0 GPa, and Poisson's ratio = 0.25. Sandstone: UCS = 80 MPa; Young's modulus E = 20 GPa, and Poisson's ratio = 0.25.

Because the massive sandstone unit is much stronger than the coal seam and is often observed to be intact after extensive failures in the coal seam, we assume that fracturing occurs only in the coal seam and no failure is allowed in the sandstone unit.

The first model was run without considering the cleats or joints in the coal seam explicitly. After the roadway excavation, fracture initiations occurred in the coal rib near the corners between the roof and floor where the stress concentration is severe. Short fractures parallel or at a small angle with the rib wall were formed (see Fig. 14). These short fractures were caused by extensional strain resulting from high compressive stress. The fractures however tended to propagate in shear and coalesce with each other to form larger fractures. The fracture initiation and propagation developed progressively deeper into the roadway ribs. Finally, a large failure zone was formed in the coal rib where the coal was extensively fractured. The depth of the failure zone was about 1.7 m.

It was noticed that the fracture propagation in the failure region was dominated by shearing although tensile fracture initiation and limited tensile fracture propagation were also involved in the process.

The second model considered two sets of short joints (cleats) in the seam, one in the vertical direction and the other in the horizontal direction (Fig. 15). The joints had a limited length and were contained in the coal mass. All other geometrical and mechanical parameters were the same as in the first model (Fig. 14). The predicted failure in the ribs started near the upper and lower corners and was mainly caused by the propagation and coalescence of the existing short joints. The failure expands deeper into the rib and toward the mid-height of the rib, eventually forming a failure zone of about 1.2 m wide in the rib. Some limited fracture propagations also occur further into the rib, but they do not appear to form any major failure.

It was observed that fractures occurring within 0.5 m from the roadway walls were caused by mixed tensile and shear failures, but deeper than 0.5 m into the rib the fracturing was mostly caused by shearing. As shear fracturing is often unstable and releases excessive strain energy, this could indicate that dynamic failure is likely to occur in roadway ribs loaded to these levels of stress.

Consistent with previous tunnel cases, the modelling results also indicated that pre-existing joints or cleats in the coal seam had reduced the intensity and the extents of rock fracturing. Compared with the case without joints (Fig. 14), the model with joints suffered less fracturing in the rib and the range of rib failure was reduced from 1.7m to about 1.2 m. Pre-existing joints or cleats can absorb some strain energy through joint deformation and sliding, and hence may be able to reduce the severity of a violent failure.

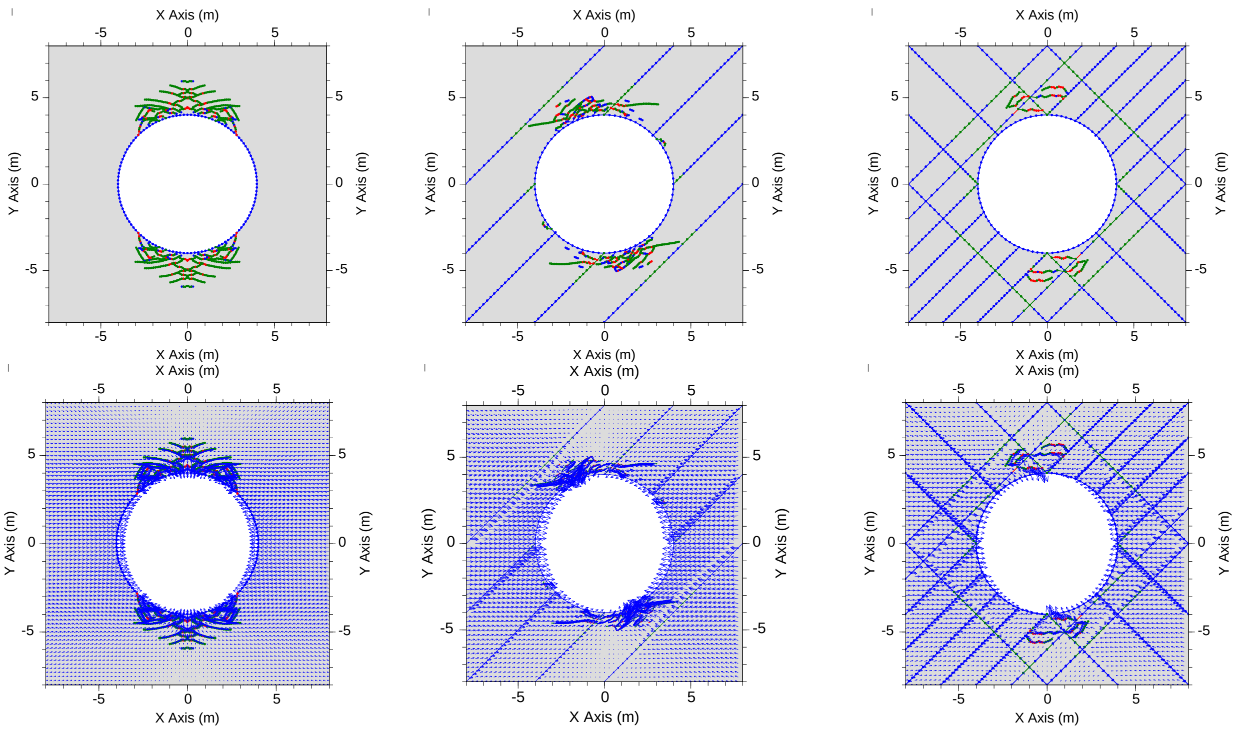

No jointing (max disp = 5.6 mm) One joint set (max disp = 6.6 mm) Two joint set (max disp = 10.4 mm)

Fig. 12 The 1,000 m depth examples. A comparison of fracturing behaviour when intact rock is replaced by rock with one or two sets of inclined jointing. Shearing along the joints is evident, and hence the much reduced fracturing of intact rock, especially when the joints are more closely spaced. Both fracturing pattern (top figures) and displacement vectors (bottom figures) are shown in the figure

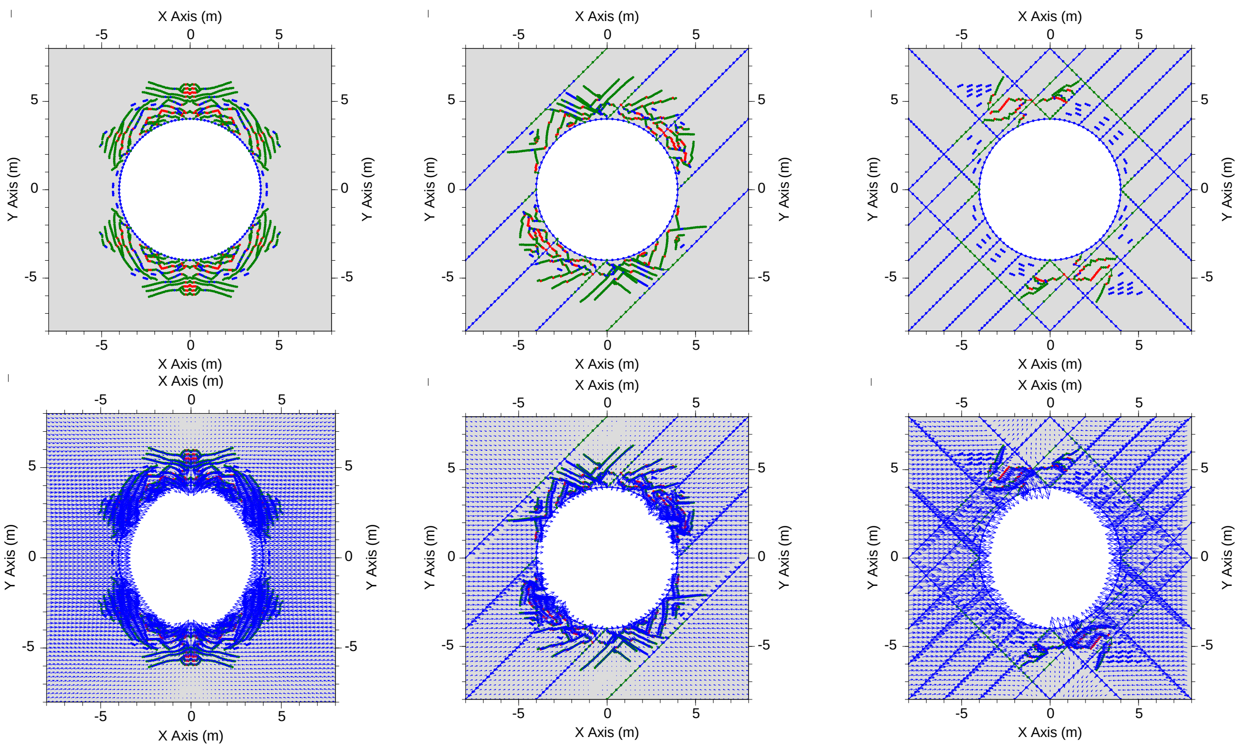

No jointing (max disp = 13.2 mm) One joint set (max disp = 22.4 mm) Two joint sets (max disp = 12.7 mm)

Fig. 13 The 2,000m depth examples. A comparison of fracturing behaviour when intact rock is replaced by rock with two sets of inclined jointing, with two different spacings. Shearing is evident, and hence the much reduced fracturing of intact rock, especially when the joints are more closely spaced. Both fracturing pattern (top figures) and displacement vectors (bottom figures) are shown in the figure

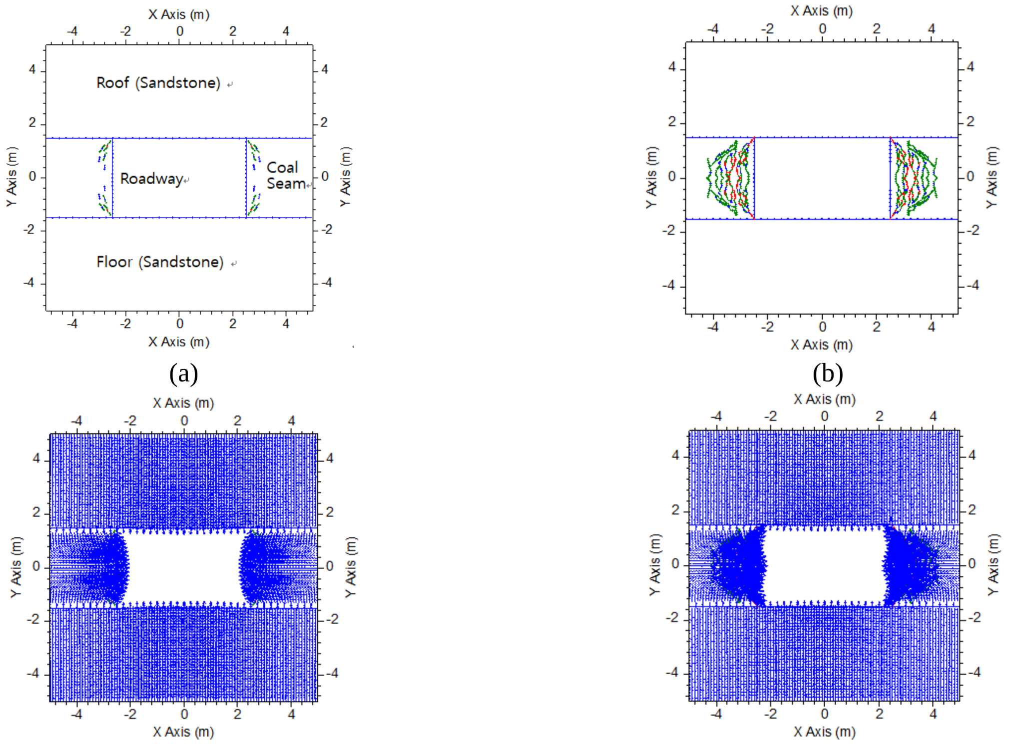

(a) (b)

(c) Max displacement = 14.1 mm (d) Max displacement = 18.3 mm

Fig. 14 Predicted failure in roadway ribs due to fracture initiation and propagation. (a) Early stage of the fracturing; (b) final stage of the failure, (c) and (d) rock displacement vectors at the two stages. The failure initially starts near the roadway corners and progresses to the centre of the coal seam. This forms the initial roadway spalling. Then new fractures initiate deeper in the rib and propagate mainly in shear, eventually forming a second 'episode' of failure

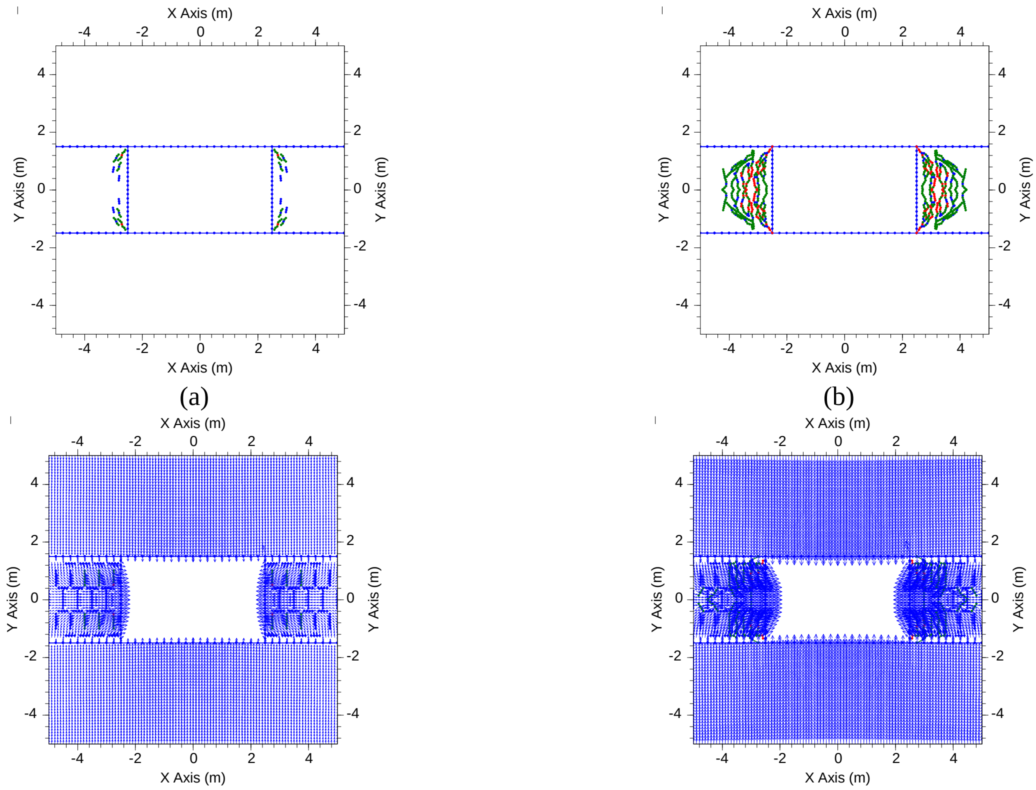

(a) (b)

(c) Max displacement = 14.2 mm (d) Max displacement = 25.2 mm

Fig. 15 Predicted failure in roadway ribs when short joints (cleats) are considered. (a) Initial status with joint system; (b) final stage of the failure, (c) and (d) rock displacement vectors at the two stages

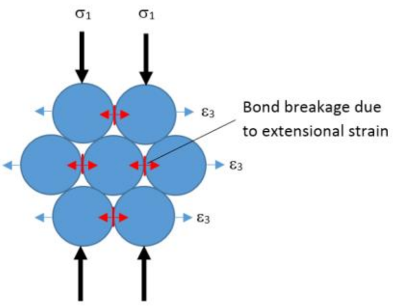

Fig. 16 Mechanism of tensile fracturing due to extensional strain caused by compressive loading

5. Discussion

The extension strain criterion, although not very new, has not yet been widely used in the rock mechanics community, yet it may hold the key to explain many phenomena such as spalling and sheeting fractures. The core concept of this criterion is that extensional strain could be caused due to compressive loading in the perpendicular direction due to the Poisson's effect. Physically, this may be understood by the mechanism shown in Fig. 16. Considering that the rock is composed of interlocked granular particles, compressive loading (σ_1) in the vertical direction tends to squeeze the particles to move horizontally, forming the "apparent" lateral deformation or extensional strain (ε_3). This lateral movement could create tension at the sub-vertical interfaces between the particles. If the loading stress is high enough, the bonds between the particles could break, creating isolated vertical tensile fractures. Note that these vertical tensile fractures may still be confined by the particles and may only be considered as fracture initiation. At this stage, rock is not yet failed in macroscale and it has not reached its peak strength. Final failure of the rock requires that these isolated tensile fractures coalesce and develop into large failure planes which may involve shear failure of some interfaces between the particles.

The above mechanism can also explain the apparent concern of some researchers that the extension strain criterion could not explain the Uniaxial Compressive Test, namely the rock specimen could fail much earlier than its uniaxial compressive strength if the extensional strain is considered. In fact, when the uniaxial load reaches approximately 0.4*UCS, only isolated tensile fractures start to develop in the rock specimen due to the lateral extensional strain, as shown in Fig. 16. This coincides with the so-called "fracture initiation" stage observed in the laboratory by many researchers, and with the commencement of Acoustic Emission (AE) events. However, these tensile fractures are short and not interlinked in the rock specimen, and therefore are not yet able to cause the rock specimen to fail. Final failure of the specimen will be formed by coalescence of the fractures at a much higher load.

The extension strain criterion may also have implication to our understanding of the Brazilian Tensile Test (BTS). Along the failure plane of the BTS disc, there exist both tensile and compressive stresses, and the compressive stress is normally three times the tensile stress. According to the extension strain criterion, the compressive stress will contribute significantly to the lateral extensional strain, which, if not accounted, could lead to an underestimation of the tensile strength of the rock. In reality however, the stress distribution along the final failure plane is very complicated, especially near the loaded ends of the specimen. Hence the interpreted tensile strength will be affected by many factors. Also note that the compression induced extensional strain may only cause fracture initiation rather than the final failure. It has been reported (e.g., Jensen 2016) that overall the tensile strength obtained by the BTS is higher than that by direct tension tests.

6. Conclusions

Rock fracturing is the key failure mechanism in underground excavations in highly stressed sparsely jointed brittle rocks. Both tensile and shear fracture initiation and propagation are likely to be involved. Fundamentally, in rock masses with high compressive stresses, tensile fracture propagation is often a stable process which leads to a gradual failure. Shear fracture propagation tends to be an unstable process and can occur violently.

Rock fracturing may occur in the vicinity of an underground opening due to the elevation of tangential stress and removal of the confining stress. Shallow spalling in the tunnel periphery (arch or wall) is believed to be caused by tensile fracturing caused by extensional strain, although no tensile stress exists there. Massive large scale failure however is most likely to be caused by shear fracturing under high compressive stresses.

The observation that tunnel spalling often starts when the maximum hoop or maximum tangential stress reaches approximately 0.4*UCS has been explained in this paper by using the extension strain criterion. At this uniaxial compressive stress level, the lateral extensional strain is equivalent to the critical strain under uniaxial tension. It is our view that a scale effect on UCS, commonly believed by many as causing the earlier than expected (0.4*UCS) micro- crack initiation and acoustic emission is not the dominant factor in this phenomenon. For rocks with a typical UCS ≈ $10\sigma_t$ and Poisson's ratio ≈ 0.25, tensile fracturing will start when the uniaxial (or tangential) stress reaches ≈ 0.4*UCS, from simple arithmetic applied in Eq. 3.

Rock fracturing and failure can be limited when one or more joint sets are present, due to shear-stress dissipation on the joints, as opposed to the need for more stress-dissipating fracturing of intact rock, in order to gain equilibrium. So *lack of jointing* could be a source of risk in deep hard-rock tunnels, whereas the presence of jointing can sometimes be a source of risk in shallow tunnels. The same principles apply to mining in hard, strong coal seams overlain by a massive sandstone unit, where energy release from fracturing cannot be adequately absorbed and hence large scale failure can be triggered.

Acknowledgements

The first author would like to thank Taishan Scholar Talent Team Plan for Advantaged and Unique Discipline

Areas, Shandong Province, for the financial support to this study.

References

Addis, M.A., Barton, N., Bandis, S.C. and Henry, J.P. (1990), "Laboratory studies on the stability of vertical and deviated boreholes", *Proceedings of the 65th Annual Technical Conference and Exhibition of the Society of Petroleum Engineers*, New Orleans, U.S.A., September .

Andersson, C. (2007), "Rock mass response to coupled mechanical thermal loading", Ph.D. Dissertation, Royal Institute of Technology, Stockholm Sweden.

Barton, N. (2006), *Rock Quality, Seismic Velocity, Attenuation and Anisotropy*, Taylor & Francis Group, London, U.K.

Barton, N. and Grimstad, E. (2014), *Q-system-an Illustrated Guide Following Forty Years in Tunnelling*, <www.nickbarton.com>.

Barton, N. and Shen, B. (2017), "Risk of shear failure and extensional failure around over-stressed excavations in brittle rock", *J. Rock Mech. Geotech. Eng.*, **9**(2), 210-225.

Cai, M. and Kaiser, P.K. (2014), "In-situ rock spalling strength near excavation boundaries", *Rock Mech. Rock Eng.*, **47**(2), 659-675.

Chen, M., Yang, S. Q., Zhang, Y.C. and Zang, C.W. (2016), "Analysis of the failure mechanism and support technology for the Dongtan deep coal roadway", *Geomech. Eng.*, **11**(3), 401-420.

Diederichs, M.S. (2003), "Rock fracture and collapse under low confinement conditions", *Rock Mech. Rock Eng.*, **36**(5), 339-381.

Diederichs, M.S., Kaiser, P.K. and Eberhardt, E. (2004), "Damage initiation and propagation in hard rock during tunnelling and the influence of near-face stress rotation", *J. Rock Mech. Min. Sci.*, **41**(5), 785-812.

Dresen, G., Stanchits, S. and Rybacki, E. (2010), "Borehole breakout evolution through acoustic emission location analysis", *J. Rock Mech. Min. Sci.*, **47**(3), 426-435.

Fairhurst, C. and Cook, N.G.W. (1966), "The phenomenon of rock splitting parallel to the direction of maximum compression in the neighbourhood of a surface", *Proceedings of the 1st Congress on the International Society of Rock Mechanics*, Lisbon, Portugal.

Grimstad, E. and Barton, N. (1993), "Updating the Q-system for NMT", *Proceedings of the International Symposium on Sprayed Concrete-Modern Use of Wet Mix Sprayed Concrete for Underground Support*, Fagernes, Norway, October.

Hoek, E. and Brown. E.T. (1980), *Underground Excavations in Rock, Institution of Mining and Metallurgy*, London, U.K., 527.

Huang H., Yang, S.Q. and Zhang, C.S. (2017), "Strength failure behavior of granite containing two holes under Brazilian test", *Geomech. Eng.*, **12**(6), 919-933.

Jensen, S.S. (2016), "Experimental study of direct tensile strength in sedimentary rocks", M.Sc. Dissertation, Norwegian University of Science and Technology, Trondheim, Norway.

Komurlu, E., Kesimal, A. and Hasanpour, R (2015), "In situ horizontal stress effect on plastic zone around circular underground openings excavated in elastic zones", *Geomech. Eng.*, **8**(6), 783-799.

Li, S.C., Wang, J.H., Chen, W.Z., Li, L.P., Zhang, Q.Q. and He, P. (2016), "Study on mechanism of macro failure and micro fracture of local nearly horizontal stratum in super-large section and deep buried tunnel", *Geomech. Eng.*, **11**(2), 919-933.

Martin, C.D. (1997), "Seventeenth Canadian geotechnical colloquium: The effect of cohesion loss and stress path on brittle rock strength", *Can. Geotech. J.*, **34**(5), 698-725.

Martin, C.D. and Chandler, N.A. (1994). "The progressive fracture of Lac du Bonnet granite", *J. Rock Mech. Min. Sci. Geomech. Abstr.*, **31**(6), 643-659.

Martin, C.D., Kaiser, P.K. and McCreath, D.R. (1999), "Hoek-Brown parameters for predicting the depth of brittle failure around tunnels", *Can. Geotech. J.*, **36**(1), 136-151.

NSW Mine Safety Investigation Unit. (2015), *Report into the Deaths of James Mitchell and Phillip Grant at the Austar Coal Mine, Paxton, NSW on 15 April 2014*, NSW Mine Safety Investigation Unit.

Read, R. and Martin, C.D. (1996), *Technical Summary of AECL's Mine-by Experiment Phase 1: Excavation Response*, Atomic Energy of Canada Ltd.

Rinne, M. (2008), "Fracture mechanics and subcritical crack growth approach to model time-dependent failure in brittle rock", Ph.D. Dissertation, Helsinki University of Technology, Espoo, Finland.

Shen, B. and Stephansson, O. (1993), "Modification of the G-criterion of crack propagation in compression", *Eng. Fract. Mech.*, **47**(2), 177-189.

Shen, B., Shi, J. and Barton, N. (2018), "An approximate nonlinear modified Mohr-Coulomb shear strength criterion with critical state for intact rocks", *J. Rock Mech. Geotech. Eng.*, **10**(4), 645-652.

Shen, B., Stephansson, O. and Rinne, M. (2014), *Modelling Rock Fracturing Processes: A Fracture Mechanics Approach Using FRACOD*, Springer, 173.

Shen, B., Stephansson, O., Einstein, H.H. and Ghahreman, B. (1995), "Coalescence of fractures under shear stresses in experiments", *J. Geophys. Res.*, **100**(B4), 5975-5990.

Siren, T. (2012), *Fracture Toughness Properties of Rocks in Olkiluoto: Laboratory Measurements 2008-2009, 2012,* Posiva Report 2012-25.

Stacey, T.R. (1981), "A simple extension strain criterion for fracture of brittle rock", *J. Rock Mech. Min. Sci. Geomech. Abstr.*, **18**(6), 469-474.

Wang, Z.S., Li, Y., Zhu, W.S., Xue, Y.G., Jiang, B. and Sun, Y.B. (2017), "Field monitoring of splitting failure for surrounding rock masses and applications of energy dissipation model", *Geomech. Eng.*, **12**(5), 595-609.

Wawersik, W.R. and Fairhurst, C. (1969), "A study of brittle rock fracture in laboratory compression experiments", *J. Rock Mech. Min. Sci. Geomech. Abstr.*, **7**(5), 561-575.

Wesseloo, J. and Stacey, T.R. (2016), "A reconsideration of the extension strain criterion for fracture and failure of rock", *Rock Mech. Rock Eng.*, **49**(12), 4667-4679.

CC